Hindawi
Advances in Materials Science and Engineering
Volume 2022, Article ID 7568553, 14 pages
https://doi.org/10.1155/2022/7568553

Research Article

Dual Input Single Phase Quasi Z Source Inverter for Integrated Photovoltaic Systems

T. Rampradesh,[1] **C. Christober Asir Rajan**,[2] **and Kinde Anlay Fante**[3]

[1]*Department of Electrical and Electronics Engineering, IFET College of Engineering, Gangarampalaiyam, Tamil Nadu, India*
[2]*Department of Electrical and Electronics Engineering, Puducherry Technological University, Puducherry, India*
[3]*Faculty of Electrical and Computer Engineering, Jimma Institute of Technology, Jimma University, Jimma, Ethiopia*

Correspondence should be addressed to Kinde Anlay Fante; kinde.anlay@ju.edu.et

Received 4 September 2022; Revised 23 September 2022; Accepted 30 September 2022; Published 22 November 2022

Academic Editor: Samson Jerold Samuel Chelladurai

Globally, climate change has increased various environmental concerns, and there is a very high and still ever greater penetration of renewable energy power into energy grids. The intermittent nature of these energy sources has demanded a strong power electronic interface to maintain an uninterrupted power flow to the external load. This paper deals with a novel dual input quasi Z source inverter (qZSI) that can operate with two intermittent sources and perform a single stage power conversion. The novelty of the proposed methodology is the implementation of qZSI with a reduced number of switches, increased voltage gain, and a high boosting factor which results in increased efficiency. A simple boost control-based pulse width modulation (PWM) technique has been adopted, which has been observed after analysis, to have reduced the stress on the switches and simultaneously increased system efficiency. Perturb and observe method-based maximum power point tracking (MPPT) was integrated into the study with the control technique, and its performance was observed using MATLAB/Simulink and further validated with a scale down model.

1. Introduction

Photovoltaic (PV) systems are certainly trendy these days, due to the large-scale implementation of solar-based power stations globally. Environmental disasters in particular have made people acutely aware of the negative consequences of using and depending upon fossil fuels as a species. So, tremendous steps have been and are still being taken, by the owners of the power generating stations to switch over to alternative energy sources [1, 2]. The challenges regarding the use of this cleaner, alternative source as a major source of energy remains its intermittent nature, as well as the low power generating capacity of the technology [3]. PV systems, after all, can operate only with an additional source of energy as well. Traditionally, batteries are used as a backup source for PV systems, as they can only operate, store, and feed extra power to loads when necessary [4]. Solar-based inverters are used as a power conditioning unit to ensure the consistency of output power, irrespective of variations in input power [5]. But even still, the efficiency of such inverters is very low.

Another important factor that affects the efficiency of a PV system is the voltage gain of the inverter and the stress on the power electronic switches used [6]. Therefore, attention towards solar inverter design and performance has gained importance too. Transformer less inverters are a major area of interest for researchers as they have some notable advantages over their counterparts, such as taking up less space, weighing less, and also increased protection [7, 8]. There are many topologies of front-end converters and load-side inverters in the literature that have specific pros and cons. Many researchers have paid attention to *Z* sources, due to their unique shoot-through capability, with which they can boost power tremendously [9–11]. Quasi Z source inverters have improved boosting capability as well as high voltage gain [12]. The switched capacitor models can operate with a lower number of switches, have high boosting capabilities, and put less stress on switches, which in turn improves the efficiency of the system [13]. Nowadays, hybrid systems are more popular in meeting the challenges of the intermittent nature of solar PV systems. Multi-input systems have been developed recently to integrate

more than one renewable energy source together, and they are found to have a better power electronic interface and bidirectional flow of power [14]. Integration of wind and solar PV systems together has a much greater efficiency in the case of grid-connected systems as well [15].

To meet the major challenge of intermittence in green energy systems, a novel dual-input quasi Z source inverter is proposed, which can operate with two different sources independently. This hybrid qZSI is designed to integrate intermittent renewable energy systems and to harvest the maximum power from the hybrid sources. A pulse width modulation (PWM) scheme based on simple boost control is adopted to control the switches, which are also interfaced with the perturb and observe (*P* and *O*) method to track the maximum available power at any instant. The proposed inverter is compared with 3 topologies of quasi Z source inverter that were proposed earlier. They were also simulated and the output voltage and current waveforms were plotted. The proposed inverter can overcome the aforementioned issues such as low output voltage, low voltage gain, high stress on switches, and low boosting capability. The design criterion mainly focuses on the integration of two sources and their independent operation. The inverter can operate with on-grid and off-grid systems effectively when compared to the existing topologies. A scale down model was developed to validate the performance.

The novelty of the proposed methodology is the implementation of qZSI with reduced number of switches, increased voltage gain, and a high boosting factor which results in increased efficiency of the overall system. The system performance is evaluated based on the boosting factor and THD level.

The segments involved in this manuscript have been structured with 7 sections. Section 2 deals with the operation of the proposed inverter under various modes using the control strategy. In Section 3, *P* and *O* method and its modelling are discussed with its flowchart and simulation results. Section 4 deals with the mathematical modelling and steady state analysis of the proposed system. The features of three different topologies of qZSI that are in literature earlier are compared with the proposed system in Section 5. Simulation results and experimental verification are performed in Sections 6 and 7, respectively.

2. Proposed Dual Input Quasi Z Source Inverter

A quasi Z source inverter is a type of impedance source inverter that can produce extended boosting capability. Like a traditional Z source inverter, the quasi Z source inverter also has passive elements and diodes. The rapid boosting of this type of inverter is achieved due to the shoot through state in which both of the switches of the same leg are turned on at the very same instant. There are many topologies of quasi Z source inverter, yet there is no single-phase quasi Z source inverter with dual input. The inverter proposed in this paper operates with a dual source, so that it can feed the load continuously at times of intermittence.

The proposed dual input qZSI is shown in Figure 1. It consists of a front end qZSI network and a switched capacitor model at the back end. Both the blocks are powered

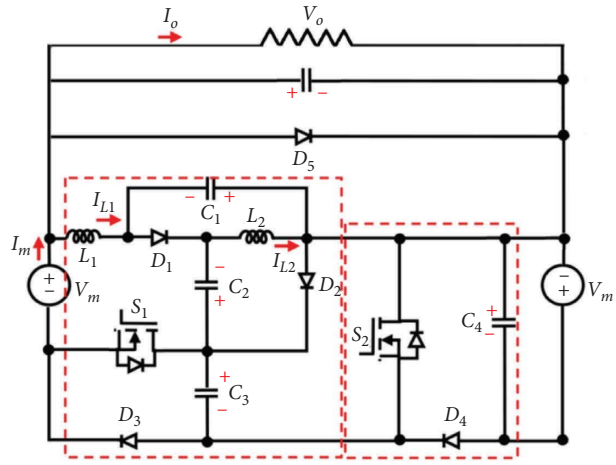

Figure 1: Dual input quasi Z source inverter.

by two individual sources $+V_{in}$ and $-V_{in}$ of opposite polarity. The quasi Z source inverter block operates to boost the power from the input source. The inductor and capacitor network feed the extra power during the shoot through mode and produce a very high boosted voltage at the output. The diodes operate the capacitors and inductors during the shoot through mode. The switch S_1 connects the source to the qZSI network at the front end. D_5 is a freewheeling diode that operates after the discharge of the capacitor and maintains the output current continuously.

The use of a switched capacitor model ensures a high boost of the input voltage and very high voltage gain during the shoot through mode of operation. Since more voltage is shared by the passive elements, the stress on the switches and the heat loss across them are reduced as well. This characteristic reduces the switching losses in the process. The two sources can operate individually and can also be fed to the load resistor as both the front and back end blocks are coupled by the passive elements. The control strategy and the associated modes of operation are discussed below.

2.1. Control Strategy. PWM based on simple boost control is adopted for its enhanced boosting capability of the inverter. We consider a PV system operating with PV and wind as major sources and a battery as a backup source. The system modeled to investigate the performance of the inverter is shown in Figure 2. There are four carrier signals CW_1, CW_2, CW_3, and CW_4, based upon which the output voltage is regulated. Here, CW_1 is fetched from the user defined value, CW_2 is fetched from the MPPT of the PV system, CW_3 is fetched from the battery voltage, and CW_4 is fetched from the other renewable energy source.

2.2. Mode 1, Front End Source Active. In this mode, the source in the front end is active. The front end consists of the impedance network, in which the boosting takes place rapidly. In this mode, while the switch S_1 is on, the flow of current is through all the passive elements and the load is fed with a high voltage and current. When the switch S_2 is on, the current flows in the back end network, i.e., capacitor C_4 is

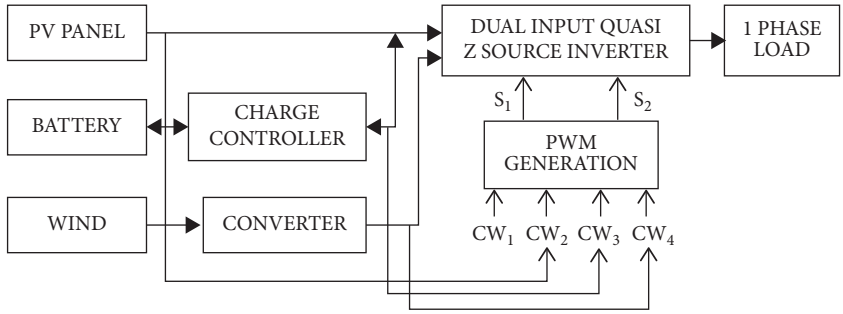

Figure 2: System to evaluate the performance of hybrid qZSI.

charged in the switched capacitor network and the load is energized. During the shoot through state, both the switches are turned on and the load is fed with a huge current while the switched capacitor is charged. The direction of the current in this mode is shown in Figure 3.

2.3. Mode 2, Back End Source Active. In mode 2, the back end source is made active. When switch S_1 is turned on, diode D_1 is reverse biased and buck operation is possible. When S_2 is turned on, both the networks are active and there is a boosted voltage to the load. During the shoot through state, both S_1 and S_2 are simultaneously on and a high current flows through the load. The capacitor is charged during this mode and the current direction is kept uniform by the freewheeling diode. The current direction in this mode of operation is shown in Figure 4.

2.4. Mode 3, Both the Sources Active. In this mode of operation, both the sources are active and the inverter is fed with its rated supply. When switch S_1 is turned on, the Z source network is active and a wide boosting of the supply power takes place. When switch S_2 is turned on, the inverter operates in the switched capacitor mode. Buck operation is possible in this mode as well. During the shoot through mode, both the sources feed the inverter with a very high voltage, and the load is fed with a tremendously high voltage. Here, the voltage gain is said to be very high and the inverter operates at maximum efficiency. The current direction in this mode of operation is shown in Figure 5.

2.5. Logical Diagram of the PWM Strategy. Simple boost control is adopted in this paper and is interfaced with the perturb (P) and observe (O) algorithm. The logical diagram is shown in Figure 6. The four-input carrier wave (CW) feeds the gates, which generate two gate pulses. CW_1, CW_2, CW_3, and CW_4 are the carrier signals which feed the inputs of the user reference value, MPP, battery, and wind power, respectively.

The switching pattern is shown in Figure 7. The gate pulse is generated by correlating two sine waveforms with a carrier triangular wave. Whenever the magnitude of the carrier wave is more, the shoot through state is achieved and when less individual switches are turned on. When CW_1 and CW_3 are in a high state, the system operates from

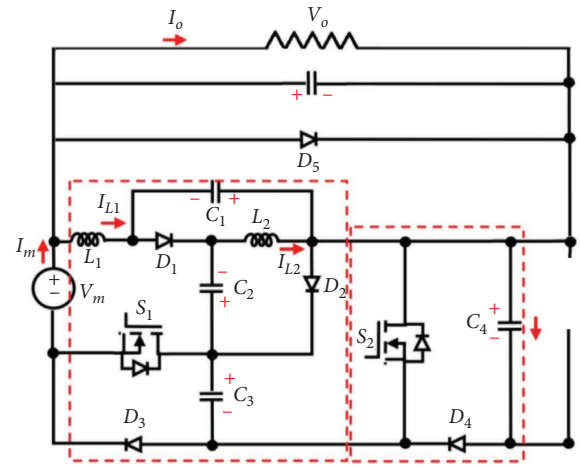

Figure 3: Operation during mode 1.

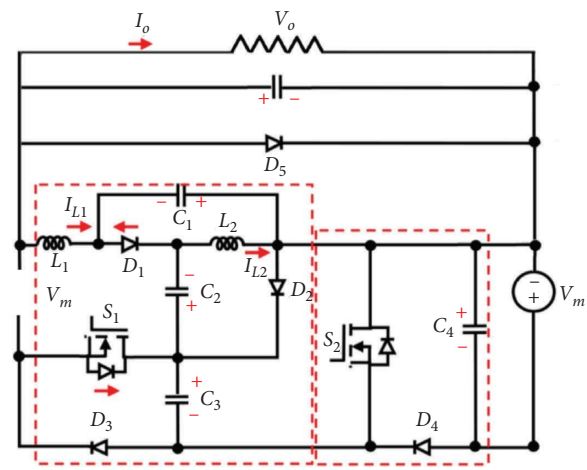

Figure 4: Operation during mode 2.

the energy delivered by the PV system alone and mode 1 is realized. If CW_4 is in a high state, the system exhibits mode 2 operation. When all three values are set to high, the system operates in mode 3. The gate pulses are complementary during buck and boost modes. During the shoot through mode, both the gate pulses have the same magnitude, and during this duration, shoot through capability is achieved. Extended boost capability is also possible in this mode. It is to be noted that in the entire mode, buck,

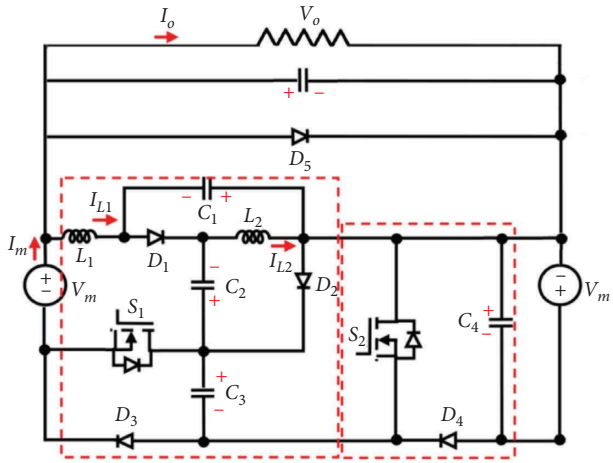

Figure 5: Operation during mode 3.

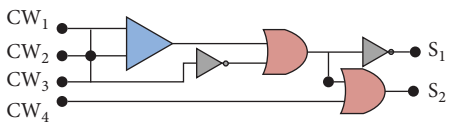

Figure 6: Logical diagram to generate gate pulses.

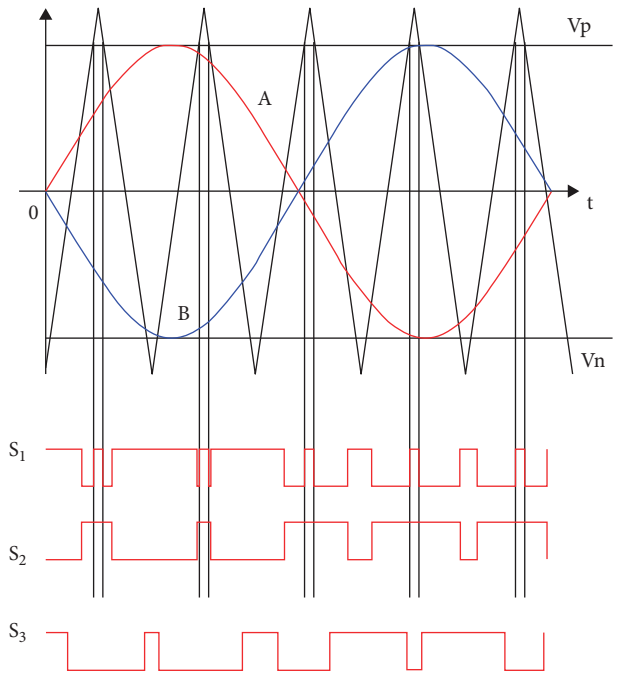

Figure 7: Simple boost switching pattern.

boost, and buck boost operations are possible. Also, the voltage gain is very high during the shoot through mode. The switching table is shown as Table 1.

3. Perturb and Observe Method

Solar power is intermittent in nature, of course. The level of insolation changes throughout the day. A specific system is required to track the maximum power that can be generated at any specific instant. Perturb and observe is a method of MPPT by which the maximum power can be tracked continuously. The method is more accurate because of its continuous tracking mechanism and the iterations are very high. A solar cell is designed with the *P* and *O* algorithm and simulated in MATLAB/Simulink. The modeled circuit is shown in Figure 8.

The current and voltage sensors sense the current and voltage at the output of the panel and feed them to the controller. The controller is programmed with a base and high value within which the panel operates. Based upon these values of voltage and current, continuous tracking of maximum power is achieved and the values are recorded. The maximum value is fed to the PWM generation circuit via CW_2. The controller then generates pulses according to the MPP, and the inverter operates in either buck or boost mode accordingly.

The P and O algorithm is interfaced in the system by the flow chart shown in Figure 9. The values of current and voltage are measured periodically. The resultant power is stored and compared with the previously obtained power. Based upon the resultant value, an error signal is generated, which triggers CW_2 and the pulse width is modified. $R(t)$ is the instantaneous value of the reference achieved from the old and new values of power. Figure 10 shows the simulation results of the proposed *P* and *O* algorithm. The variation of the duty cycle with respect to the change in the output voltage and the marginal changes of irradiance to that of the temperature is clearly depicted from the figure.

4. Steady State and Mathematical Analysis

By applying Kirchoff's voltage law to Figure 5, the equations for the voltage can be expressed as

$$V_{L2} = -V_{in} + V_{C4}, \tag{1}$$

$$V_{L1} = V_{in} + V_{C2} + V_{C3} + V_{C1}, \tag{2}$$

$$V_{C01} = V_{C2} + V_{C3} - V_{C4} - V_{L2} + V_{in}, \tag{3}$$

$$V_{CO2} = V_{in} + V_{C3} - V_{C1} - V_{C4} - V_{L2}, \tag{4}$$

$$V_{C03} = V_{in} + V_{C2} + V_{C1} - V_{C4} - V_{L2}, \tag{5}$$

$$V_{C04} = V_{in} + V_{L2} - V_{L1} - V_{C1} - V_{C2} - V_{C3}, \tag{6}$$

$$V_0 = V_{C1} + V_{C2} + V_{C3} + V_{C4}. \tag{7}$$

By applying the voltage second principle and the equations from (1) to (7), the voltage gain versus duty cycle can be obtained as

$$V_{C1} = \frac{1-D}{1-2D} V_{in}, \tag{8}$$

$$V_{C2} = \frac{1-D}{1-2D} V_{in}, \tag{9}$$

Table 1: Switching table.

	Active source	Boost operation	Buck operation	Shoot through mode
Mode 1	Front end	S_1	S_2	S_1, S_2
Mode 2	Back end	S_2	S_1	S_1, S_2
Mode 3	Both	S_1, S_2	S_2	S_1, S_2

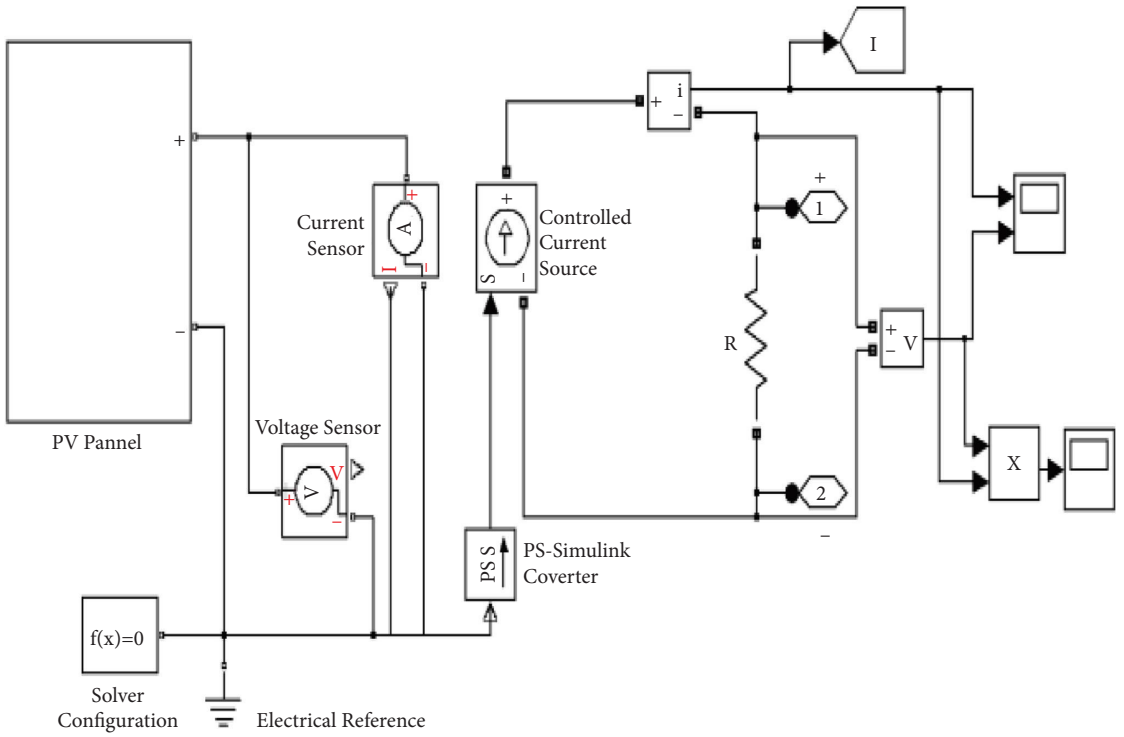

Figure 8: Model of the P and O block in MATLAB/Simulink.

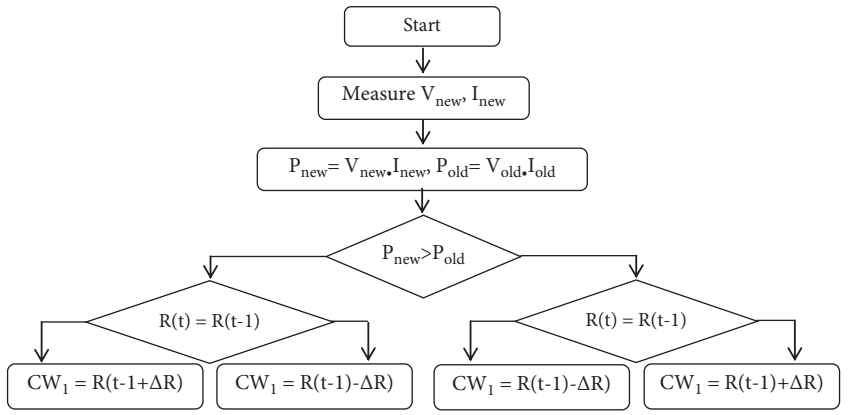

Figure 9: Flow chart for the P and O method.

$$V_{C3} = \frac{V - D}{1 - 2D} V_{in}, \tag{10}$$

$$V_{C4} = \frac{V - D}{1 - 2D} - V_{in}. \tag{11}$$

Substituting the equations (8) to (11) in the voltage equations and applying coupled inductor turns ratio ($N_2/N_1 = n$) and coupling coefficient k, the voltage across the capacitors can be given as

$$V_{C01} = \frac{1}{1 - 2D} V_{in}, \tag{12}$$

$$V_{C02} = \frac{1 + nk - D(n - 1)}{1 - 2D}, \tag{13}$$

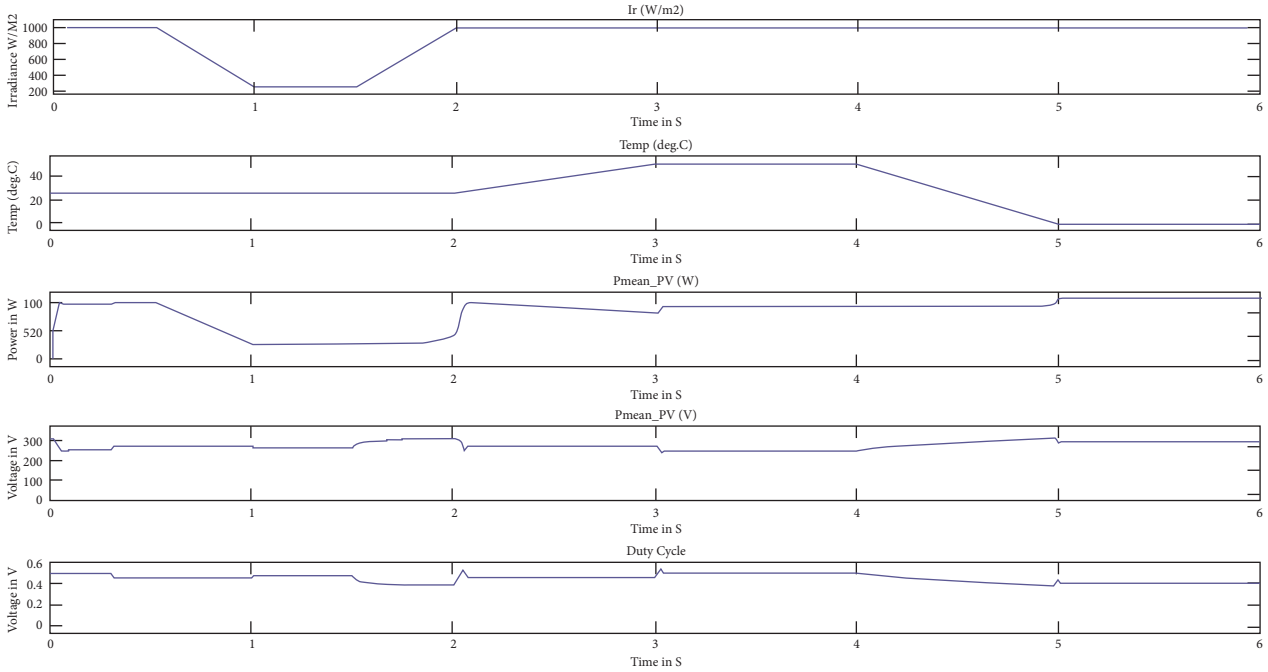

Figure 10: Output graphs of the proposed *P* and *O* method.

$$V_{C03} = \frac{nk - (1+D)}{1-D} V_{in}, \tag{14}$$

$$V_{C04} = \frac{nk(1+D)}{1-D} - V_{in}, \tag{15}$$

$$V_0 = \frac{2 + nk(2-D)}{1-D} - V_{in}. \tag{16}$$

Ignoring leakage reactance and assuming $k = 1$, the voltage gain is given by

$$G = \frac{V_0}{V_{in}} = \frac{2 = n(1-D)}{1-2D}. \tag{17}$$

In addition to the capacitors, the associated voltage stress on the switches can be found by

$$M_S = M_{D1} = M_{D2} = M_{D3} = \frac{(2G+n)}{G(3n+1)}, \tag{18}$$

$$M_{D0} = M_{D4} = \frac{(1+n)(2G+n)}{G(3n+1)}, \tag{19}$$

$$M_{D5} = \frac{(2G-n)}{2G(3n+4)}. \tag{20}$$

$M_S = V_S/V_0$ is the voltage stress on the switch and $M_D = V_D/V_0$ is the voltage stress on the diode.

By using Ampere second balance principle, the stress on the switches can be calculated as

$$i_s = \frac{1 + 2n - (1-n)D}{1-D} I_0, \tag{21}$$

$$i_{D1} = \frac{2 + 2n - D}{(1-D)(1-2D)} I_0, \tag{22}$$

$$i_{D2} = i_{CO_2-off} - i_{CO1off} = \frac{1}{1-2D} I_0, \tag{23}$$

$$i_{D3} = i_{CO_3-on} = \frac{1}{2D} I_0, \tag{24}$$

$$i_{D4} = i_{CO_4-on} = \frac{1}{1-D} I_0, \tag{25}$$

$$i_{DO} = i_{C_3-off} = \frac{1}{1-D} I_0. \tag{26}$$

5. Comparison Study

Quasi Z-source inverters have been discussed in the literature since 2011. Since then, there have been many new topologies of quasi Z source inverters. Yet, a topology with a dual input is very rare in the literature. In addition, no single-phase dual input qZSI had been published in the literature. Dual input can always serve in times of intermittence of renewable energy systems and aids in the

efficient handling of sources with less overall stress on the switches of a system. Here, a few dual input quasi Z source inverters are compared with the proposed inverter. A dual input PV inverter was proposed in [16], which can produce two DC and one AC output. A multi-input, multi-output inverter was introduced in [17] whose dynamic response is fast. A cascaded type multilevel inverter was proposed in [18] which has a high boosting capability. A comparison in terms of the number of components, phase, and boost factors is shown in Table 2 and it is to be noted that the boost factor of the proposed inverter is high compared to its counterparts.

6. Simulation

The system comprising the dual input hybrid quasi Z source inverter in Figure 2 was simulated in the MATLAB/Simulink environment. Three different conditions are taken into consideration to plot the characteristics and depict the three modes of operation in this simulation.

To plot the characteristics of mode 1, the voltage from the PV alone was considered. Now, the front-end network alone was powered and the boost operation was performed. Figure 11 shows the output voltage and current waveforms for mode 1. For an input of 50 V, the system generated an output of 100 V.

The characteristics of mode 2 were simulated by removing the PV power and activating the wind power alone. In this case, the back end network was fully powered and the output voltage was boosted. Figure 12 shows the output voltage and current waveforms for mode 2. When an input of 75 V was fed, the inverter boosted it to 150 V.

Mode 3 characteristics were plotted by activating both the sources. Now, there is a very high boost in voltage and continuous current is obtained. When the two sources were powered by 50 V and 50 V, respectively, the system fed the load with 200 V. The output waveforms are shown in Figure 13. The various input and output voltages are shown in Table 3.

FFT analysis of the waveform was performed in MATLAB to measure the total harmonic distortion (THD). The bar chart of the magnitude of the fundamental frequency vs the harmonic order is shown in Figure 14. The THD value was 24.15% with an LC filter connected across the load. The low THD value is because of the lower stress and the minimal number of switches. Also, the passive elements carry the maximum voltage and the THD value is found to be considerably low.

The proposed PWM-based simple boost controller was used to test the performance of its counterparts, and the voltage and current waveforms were obtained with the same input voltages as that of the proposed topology. The topology proposed in [16] produced an output voltages of 40 V, 60 V, and 90 V for input voltages of 50 V, 75 V, and 100 V, respectively. The corresponding voltage and current waveforms are shown in Figure 15.

The output waveforms for the topology proposed in [17] are shown in Figure 16. The output voltages are 60 V, 85 V, and 120 V for an input voltage of 50 V, 75 V, and 100 V, respectively.

The voltage and current waveforms for the topology proposed in [18] are shown in Figure 17. The inverter boosted an input voltage of 50 V, 75 V, and 100 V to 65 V, 100 V, and 130 V, respectively.

The output voltages for various inputs are tabulated in Table 4 and the comparison chart is shown in Figure 17. The proposed topology has shown a significant rise in the output voltages compared to its counterparts.

The inference from the comparative chart of the voltage profile from Figure 18 is that, the topologies proposed in [16] are seen to operate in buck mode for all the three different input voltages. The topology proposed in [17] is seen to operate in buck mode for an input voltage of 50 V and boost mode for an input voltage of 75 V and 100 V. However, the voltage gain is not large compared to the proposed inverter. The topology proposed in [18] has shown a boost mode of operation for all three different types of input voltages. For an input voltage of 50 V, 75 V, and 100 V, the inverter gave an output voltage of 65 V, 100 V, and 130 V, respectively, with a voltage gain of 1.3.

The proposed inverter has produced an output voltage of 100 V, 150 V, and 200 V for an input voltage of 50 V, 75 V, and 100 V, respectively. The voltage gain is 2 for the proposed inverter which is very high and also has reduced number of switches. The boosting factor is also very high compared to its counterparts and is more reliable for intermittent sources.

7. Experimental Verification

The system performance was experimentally verified regarding both buck and boost operations with a scale down model shown in Figure 19, which was developed in the laboratory. The system was powered by a battery, a PV panel, and a small wind power system. A wind power module with a capacity of 50 W was used, and a solar PV training module of 500 W was used to realize the solar PV array. A battery bank of 12 V, 3 Ah capacity was used as a backup source. The wind speed and the PV output were varied, and the inverter was fed with different voltages and the output voltage was noted.

The output voltage curve for an input voltage of 50 V fed by the PV and battery into $+V_{dc}$ is shown in Figure 20 and the value of the output voltage was 100 V.

The output voltage of the wind and battery was boosted using a chopper and was fed at 75 V. The overall voltage through $-V_{dc}$ was 75 V and the output voltage of the inverter was found to be 150 V. The output voltage characteristic is shown in Figure 21.

Furthermore, both the PV and wind were energized sufficiently to feed the system with a net input voltage of 100 V and the performance of the inverter was tested. The inverter gave an output voltage of 200 V and the characteristics are shown in Figure 22.

The values of the voltage levels during the experiment, using a laboratory prototype, are shown in Table 5. It is evident from the characteristics that the inverter adapts itself to the variation in the input voltages and boosts the voltage consistently to a minimum value of 50%.

Table 2: Comparison study.

Category	[16]	[17]	[18]	Proposed topology
Switches	6	4	4	2
Capacitors	3	2	4	5
Inductors	2	2	2	2
Diode	1	1	1	4
Phase	3	1	1	1
No of input	2	2	1	2
Boost factor	$1 - D/1 - 2D$	$D/1 - 2D$	$1 - D/1 - 2D$	$1 - D/1 - 2D - D^2$

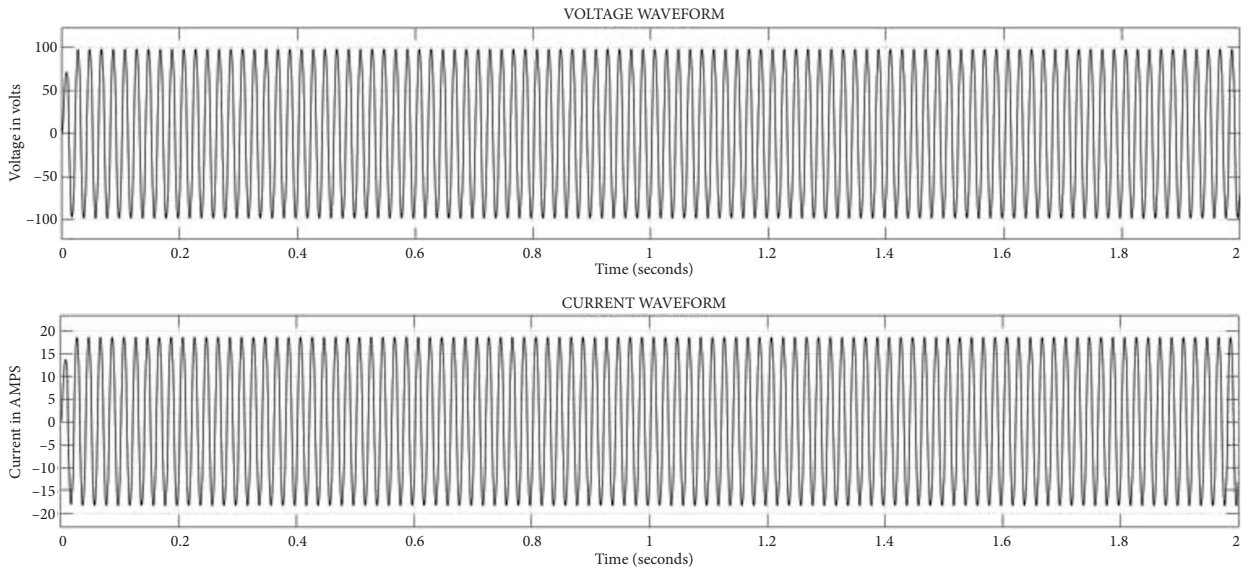

Figure 11: Output waveform during mode 1.

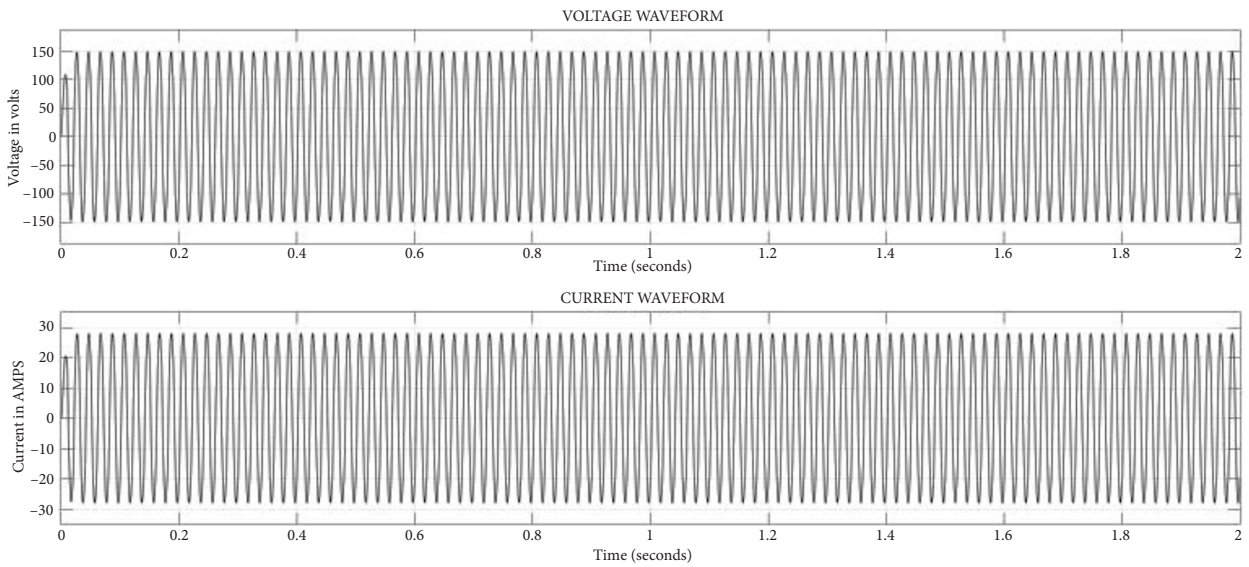

Figure 12: Output waveform during mode 2.

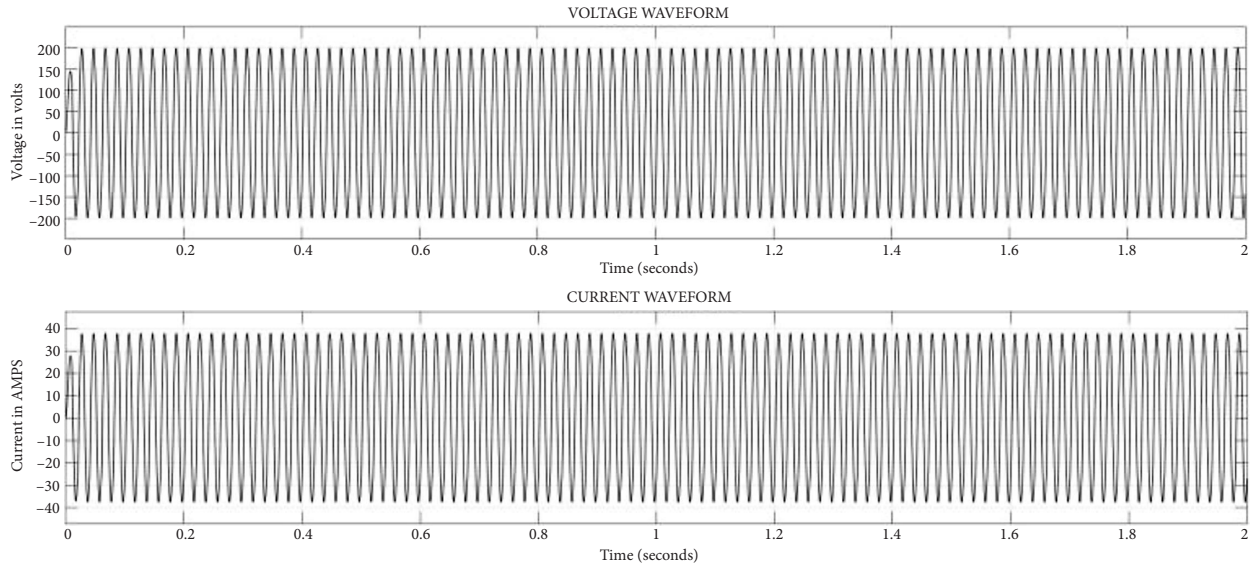

Figure 13: Output waveform during mode 3.

Table 3: Input and output voltages for various modes of operation.

Sl. No.	Mode	Input voltage in volts		Output voltage in volts
		Front end	Back end	
1	Mode 1	50	*	100
2	Mode 2	*	75	150
3	Mode 3	50	50	200

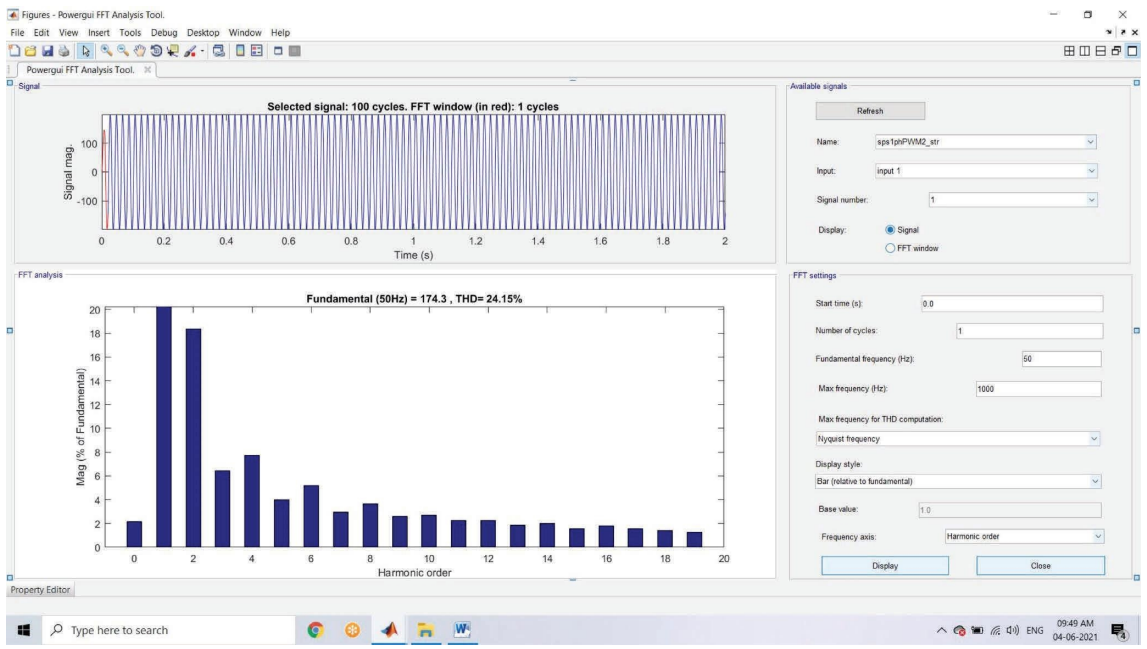

Figure 14: Total harmonic distortion.

7.1. Discussion. It is observed from the simulation and experimental results that, there is a drastic boost of the input voltages under various modes of operation of the proposed converter. Both in simulation and experimental results, the voltage gain is double and that the output voltage is double to that of the summation of the input voltages. The proposed control strategy and MPPT algorithm has worked effectively to maintain the output voltage constant irrespective of the

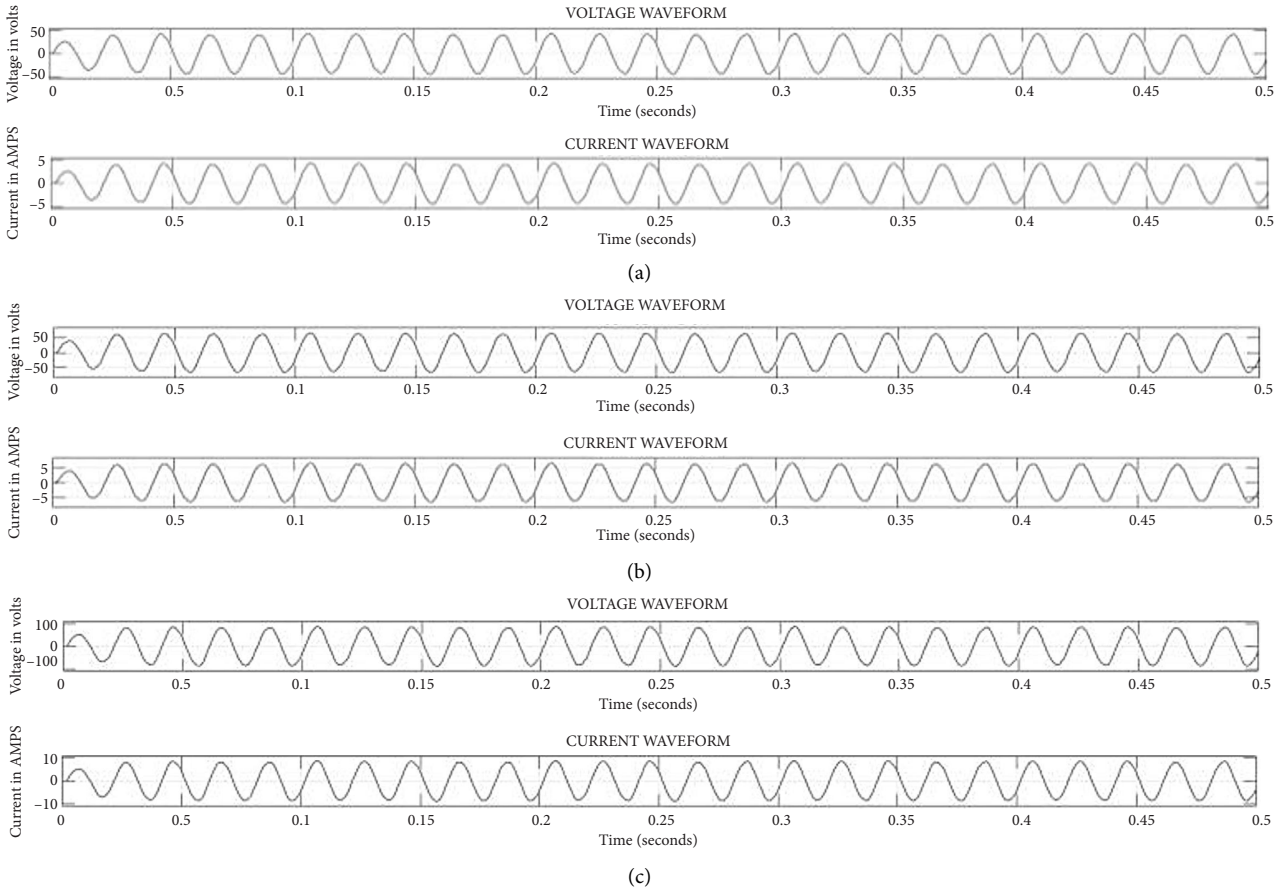

Figure 15: Output waveforms [16]. (a) Output waveforms for 50 V input. (b) Output waveforms for 75 V input. (c) Output waveforms for 100 V input.

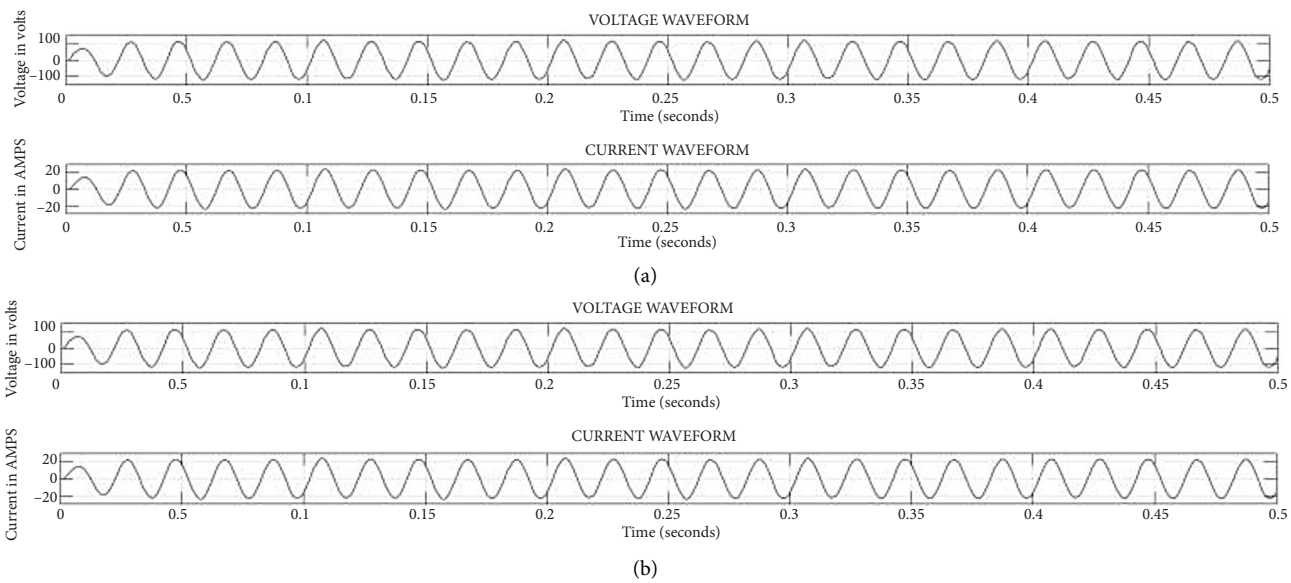

Figure 16: Continued.

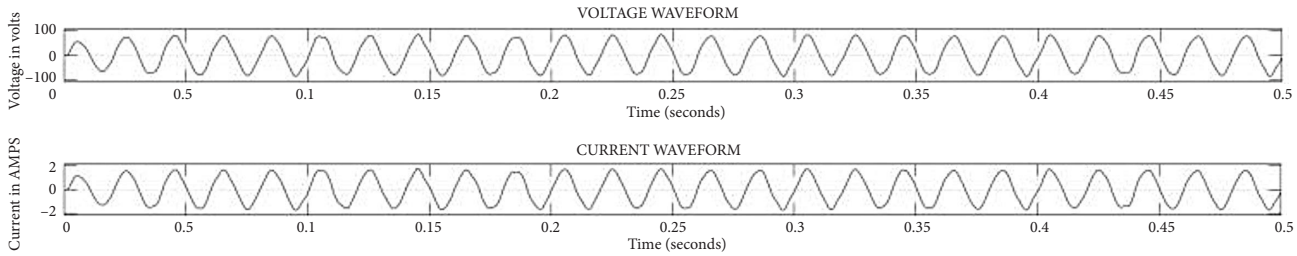

(c)

Figure 16: Output waveforms [17]. (a) Output waveforms for 50 V input. (b) Output waveforms for 75 V input. (c) Output waveforms for 100 V input.

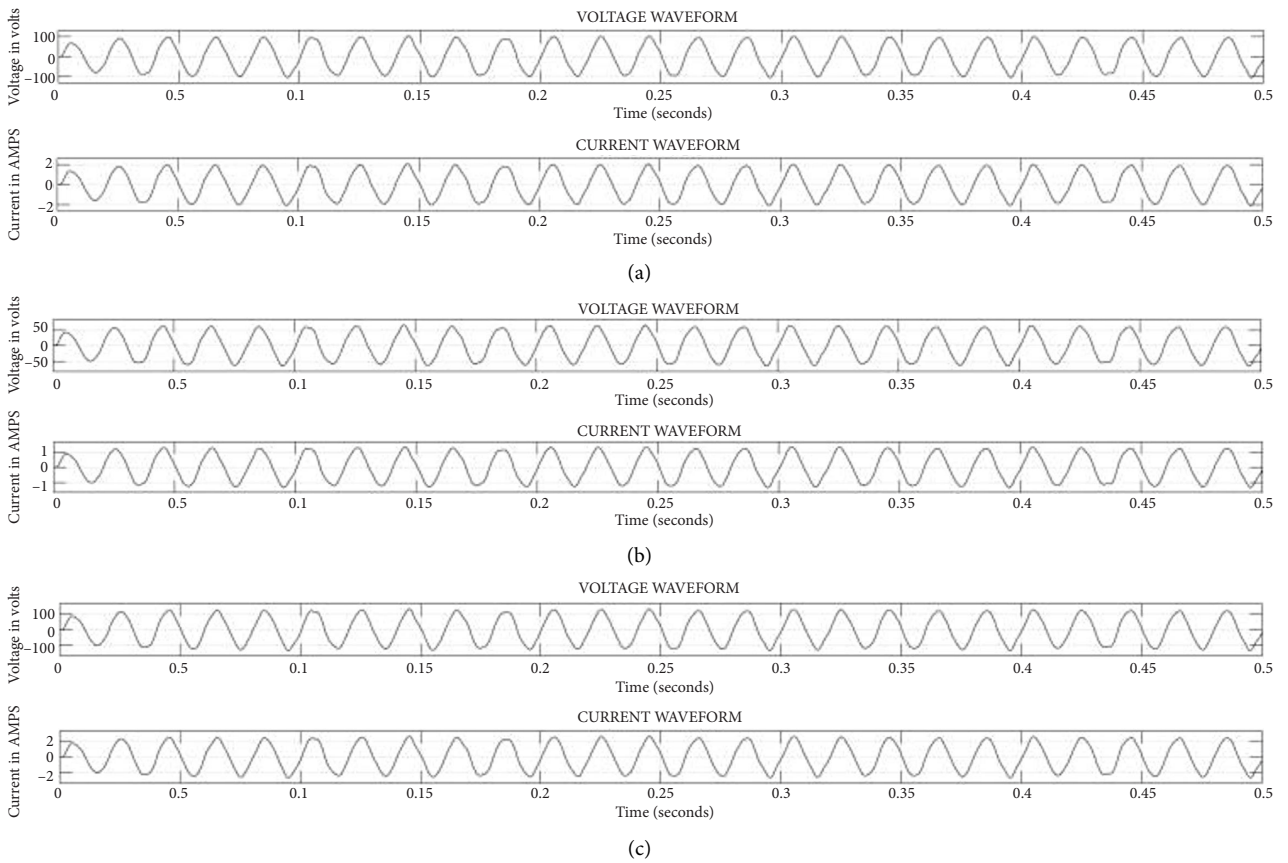

(a)

(b)

(c)

Figure 17: Output waveforms [18]. (a) Output waveforms for 50 V input. (b) Output waveforms for 75 V input. (c) Output waveforms for 100 V input.

Table 4: Comparison of output voltages for various topologies.

Input voltage (V)	Lashab et al., 2020 [16] (V)	Bagheri et al., 2020 [17] (V)	Ho et al., 2018 [18] (V)	Proposed topology (V)
50	40	60	65	100
75	60	85	100	150
100	90	120	130	200

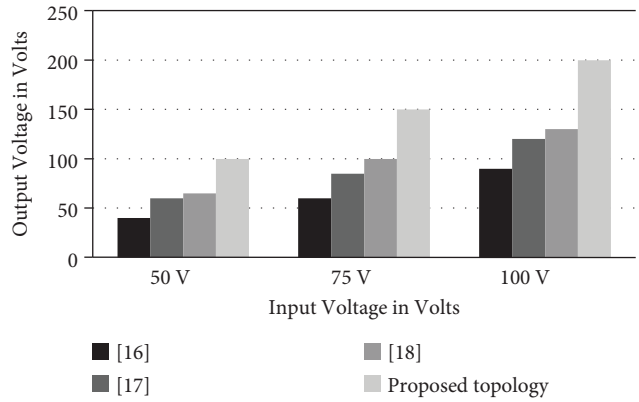

Figure 18: Comparison of output voltages of various topologies.

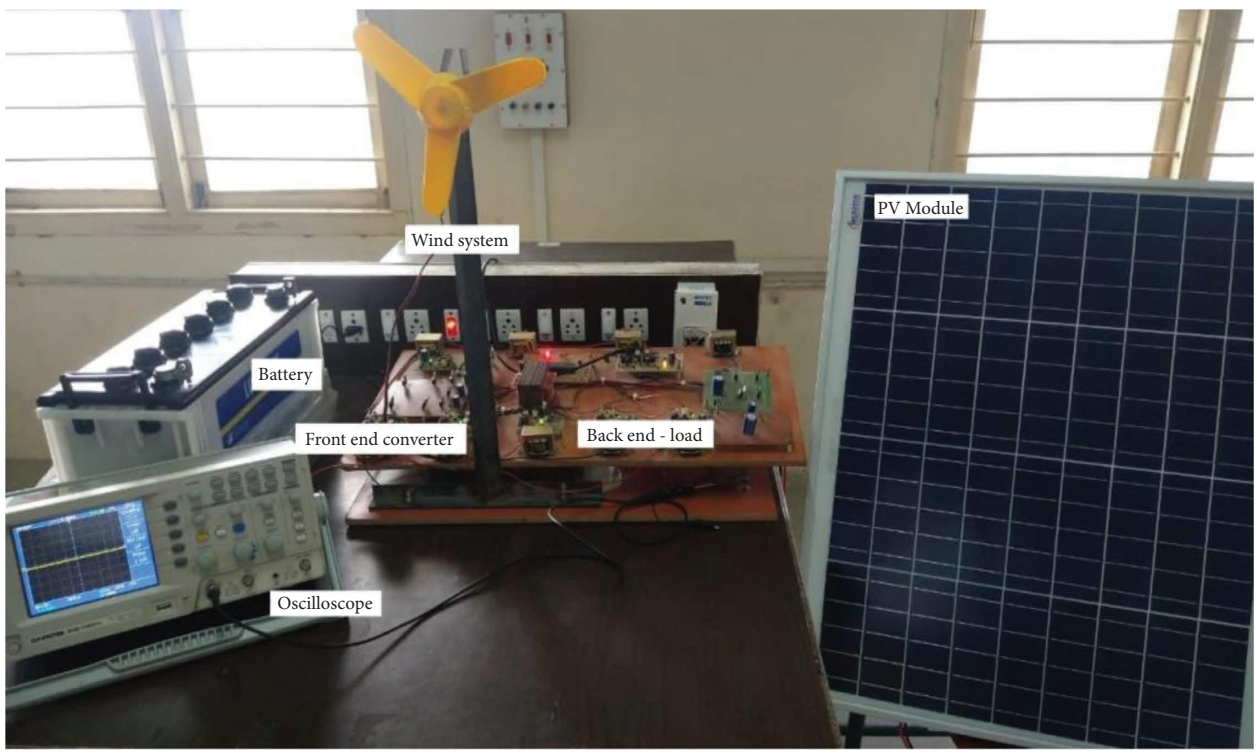

Figure 19: Experimental setup.

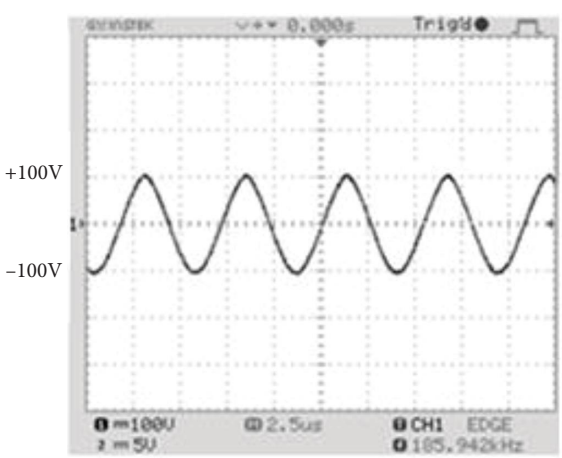

Figure 20: Output voltage waveform when $+V_{dc} = 50$ V.

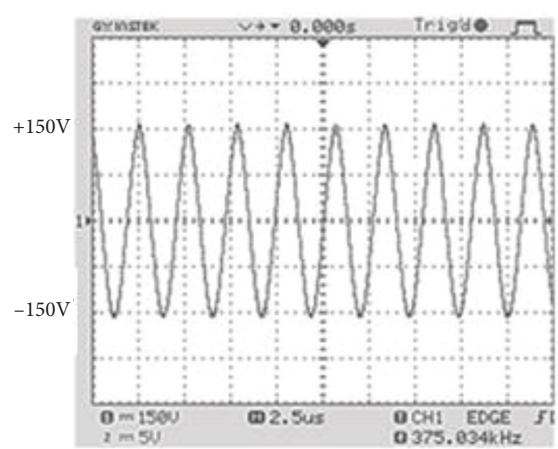

Figure 21: Output voltage waveform when $-V_{dc} = 75$ V.

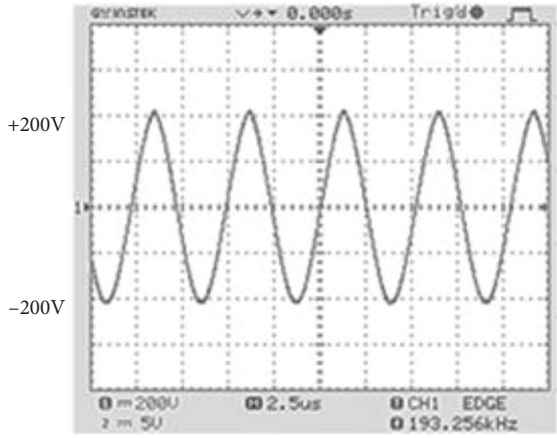

Figure 22: Output voltage waveform when $V_{dc} = 100$ V.

Table 5: Inferences from the voltage characteristics in experiment.

Input voltage	Output voltage	
	Boost mode	Buck mode
50 V	100 V	*
75 V	*	150 V
100 V	200 V	*

variations of the input voltages obtained from solar and wind. The THD value is also considerably low compared to the previous converters, and the reduced number of switches has contributed to increased efficiency of the system.

8. Conclusions

The issue of intermittence that was existing in the renewable energy power generation is overcome by the proposed, single phase dual input hybrid quasi Z source inverter with reduced number of switches and was simulated and the output waveforms were plotted by designing a real-time PV-wind integrated system. The *P* and *O*-based MPPT algorithm was modeled and the various output waveforms were plotted for the various modes of operation. The output waveforms depict that the proposed dual input qZSI has a high voltage gain and enhanced boosting capability. The boost factor is doubled and the efficiency is increased by 50% compared to that of their counterparts due to the reduced number of switches. The PWM technique adopted in this system was adaptable to MPPT and was able to operate in the shoot through state in all three modes of operation. FFT analysis shows a low THD value. Also, the harmonic order is lower. However, the first harmonic is high and can be reduced by designing a suitable filter. The results from the laboratory prototype have shown enhanced values of voltage gain. The intentional variation in the input has shown considerable changes in the output as well as in the experimental setup. In comparison with its counterparts, the proposed inverter has proven to be very effective in terms of component count and boosting factor. In comparison with the simulation results of the existing topologies, the proposed inverter has a higher voltage gain. Therefore, the proposed inverter can be used in places of high intermittence and large load requirements.

Nomenclature

V_{L2}: Voltage across inductor L_2
V_{L1}: Voltage across inductor L_1
V_{C1}: Voltage across capacitor C_1
V_{C2}: Voltage across capacitor C_2
V_{C3}: Voltage across capacitor C_3
V_{C01}: Total voltage discharged across capacitor C_1
V_{C02}: Total voltage discharged across capacitor C_2
V_{C03}: Total voltage discharged across capacitor C_3
V_{C04}: Total voltage discharged across capacitor C_4
D: Boost factor
G: Voltage gain
M: Voltage stress
V_{new}: Instantaneous voltage
I_{new}: Instantaneous current
P_{new}: Instantaneous power.

Data Availability

The data used to support the findings of this study are included within the article.

Conflicts of Interest

The authors declare that there are no conflicts of interest regarding the publication of this paper.

References

[1] A. K. Singh, S. Kumar, and B. Singh, "Solar PV Energy Generation System interfaced to three phase grid with improved power quality," *IEEE Transactions on Industrial Electronics*, vol. 67, no. 5, pp. 3798–3808, 2020.

[2] S. Singh, S. Kewat, B. Singh, B. K. Panigrahi, and M. K. Kushwaha, "Seamless control of solar PV grid interfaced system with Islanding Operation," *IEEE Power and Energy Technology Systems Journal*, vol. 6, no. 3, pp. 162–171, 2019.

[3] W. Liang, Y. Liu, and J. Peng, "A Day and Night-OperationalQuasi-Z SourceMultilevelGrid-Tied PV Power-System to Achieve active and reactive power control," *IEEE TransactionsonPowerElectronics*, vol. 36, no. 1, pp. 474–492, 2021.

[4] S. Shubhra and B. Singh, "Three-phase grid-interactive solar PV-battery microgrid control based on normalized gradient adaptive regularization factor neural filter," *IEEE Transactions on Industrial Informatics*, vol. 16, no. 4, pp. 2301–2314, 2020.

[5] P. Ponnusamy, P. Sivaraman, D. J. Almakhles et al., "A new multilevel inverter topology with reduced power components for domestic solar PV applications," *IEEE Access*, vol. 8, no. 8, pp. 187483–187497, 2020.

[6] H. Jafarian, S. Bhowmik, and B. Parkhideh, "Hybrid current-voltage-mode control scheme for distributed AC-stacked PV inverter with low-bandwidth communication requirements," *IEEE Transactions on Industrial Electronics*, vol. 65, no. 1, pp. 321–330, 2018.

[7] M. Meraj, S. Rahman, A. Iqbal, and N. Al Emadi, "Novel LevelShifted PWM TechniqueforUnequal and Equal-PowerSharing in Quasi Z-SourceCascadedMultilevelInverterfor PV systems," *IEEE Journal of Emerging and SelectedTopics in PowerElectronics*, vol. 9, no. 1, pp. 937–948, 2021.

[8] X. Huang, X. Ruan, L. Zhang, and F. Liu, "Second harmonic current Reduction schemes for DC–DC converter in two-stage PFC converters," *IEEE Transactions on Power Electronics*, vol. 37, no. 1, pp. 332–343, 2022.

[9] O. Husev, D. Vinnikov, C. Roncero-Clemente, A. Chub, and E. Romero-Cadaval, "Single-PhaseString solar qZS-basedInverter: Example of multi-ObjectiveOptimizationDesign," *IEEE TransactionsonIndustryApplications*, vol. 57, no. 3, pp. 3120–3130, 2021.

[10] M. Mohammadi, J. S. Moghani, and J. Milimonfared, "A novel dual switching frequency modulation for Z-source and Quasi-Z-Source Inverters," *IEEE Transactions on Industrial Electronics*, vol. 65, no. 6, pp. 5167–5176, 2018.

[11] F. Liu, X. Ruan, X. Huang, Y. Qiu, and Y. Jiang, "Control scheme for reducing second harmonic current in AC–DC–AC converter system," *IEEE Transactions on Power Electronics*, vol. 37, no. 3, pp. 2593–2605, 2022.

[12] T. Li and Q. Cheng, "A comparative study of Z-source inverter and enhanced topologies," *CES Transactions on Electrical Machines and Systems*, vol. 2, no. 3, pp. 284–288, 2018.

[13] X. Ding, K. Li, Y. Hao, H. Li, and C. Zhang, "Family of theCoupled-inductor MultiplierVoltageRectifierQuasi-Z-SourceInverters," *IEEE Transactions on Industrial Electronics*, vol. 68, no. 6, pp. 4903–4915, 2021.

[14] E. S. Oluwasogo and H. Cha, "A Quadratic Quasi-Z-source Full-Bridge Isolated DC–DC converter with high Reliability for wide input applications," *IEEE Transactions on Industrial Electronics*, vol. 69, no. 10, pp. 10090–10100, 2022.

[15] M. Zhang, H. Li, Y. Hao, K. Li, and X. Ding, "A Modified-Switched-coupled-InductorQuasi-Z-SourceInverter," *IEEE Journal of Emerging and SelectedTopics in PowerElectronics*, vol. 9, no. 3, pp. 3634–3646, 2021.

[16] A. Lashab, D. Sera, J. Martins, and J. M. Guerrero, "Dual-input Quasi-Z-source PV inverter: dynamic modeling, design, and control," *IEEE Transactions on Industrial Electronics*, vol. 67, no. 8, pp. 6483–6493, 2020.

[17] F. Bagheri, H. Komurcugil, O. Kukrer, N. Guler, and S. Bayhan, "Multi-input multi-output-based sliding-mode controller for single-phase Quasi-Z-source inverters," *IEEE Transactions on Industrial Electronics*, vol. 67, no. 8, pp. 6439–6449, 2020.

[18] A. V. Ho and T. W. Chun, "Single-phase modified Quasi-Z-Source cascaded hybrid five-level inverter," *IEEE Transactions on Industrial Electronics*, vol. 65, no. 6, pp. 5125–5134, 2018.